Design considerations for complementary inchworm® actuators

Shaun P. Salisbury, David F. Waechter, *Member, IEEE*, Ridha Ben Mrad, *Member, IEEE*, S. Eswar Prasad, Richard G. Blacow, and Bin Yan

Abstract— **An inchworm actuator is described which uses complementary configurations for the two clamping sections. In one configuration, clamping and release are achieved using high and low voltage respectively while for the other clamping and release are achieved using low and high voltage respectively. The resulting inchworm actuator can be driven by a two-channel controller with the two clamps sharing the first channel and the extender piezoelectric actuator using the second channel. The paper also describes a diode-shunted delay circuit that causes unclamping to occur more slowly than clamping. It is shown that by using the delay circuit in series with each clamp, the overall force drive capability of the actuator is increased. The paper presents simulated and experimental results of clamp force vs. time during the switching transient. An analysis of a generalized delay circuit having both resistive and reactive elements shows that a purely resistive design provides the better tradeoff between increased force drive capability and power loss in the delay circuit.**

Index Terms— **actuator, complementary, inchworm, piezoelectric**

I. INTRODUCTION

INCHWORM actuators are devices that achieve long range motion by rapidly repeating a clamp-extend-clamp cycle[1]. They typically use two piezoelectric actuators for two clamp sections and a third for the extender section[2]. Magnetostrictive[3], electrostrictive[4] or electrostatic[5] actuation have also been proposed for the clamp or extender sections. In the coarse positioning mode, the clamp and extender sections are activated in the required sequence by a 3-channel controller. A fine positioning mode can also be realized by activating the extender section under continuous feedback control while one clamp is on and the other is released [2].

While hybrid inchworm actuators have been proposed in which the clamp and extender sections use different actuation technologies[3], it is most often the case that the two clamp sections use the same actuation technology in an identical configuration. In this work, we examine the use of complementary clamps in which one clamp grips with low voltage and releases with high voltage while the other grips with high voltage and is released with low voltage. These will be referred to as normally clamped (NC) and normally unclamped (NU) respectively. Complementary clamps make it possible to drive the inchworm actuator with a 2-channel controller with the two clamps sharing a common channel[6]. It is also possible to enter the fine positioning mode with both clamps unpowered. The paper also describes a diode-shunted resistive circuit, which when placed in series with each clamp, slows the rate of unclamping relative to clamping. The circuit is used in order to increase the total restraining force of the two clamps during the switching transient, thereby increasing the overall force drive capability of

the actuator.

This paper presents a complementary inchworm design, delay circuit for improving total restraining force, and a simulation model-based design tool which is validated through experimental work. Section II describes the general concept of complementary inchworm actuation and introduces some clamp designs with adjustable clamping thresholds. Section III describes the delay circuit and explains its operation. Section IV then presents the dynamic model used in simulations and Section V presents experimental results. In Section VI, the simulation validation results and analysis are presented. Conclusions are summarized in Section VII.

II. ACTUATOR CONCEPT

A general configuration of a linear complementary inchworm actuator is shown in Fig. 1. The actuator has one NC and one NU type clamp. Either may be stationary but when high speed is required, the clamp type with the smaller mass is normally used as the moving clamp. The extender actuator separates the two clamps and a spring mechanism returns it to the original position when the extender is de-energized. In the configuration shown, the body of the actuator is fixed and a plate termed the moving member performs the motion. The disadvantage of the mobile NU clamp is that during fine positioning, the clamp signal must be at high voltage. If the NC clamp is mobile, then fine positioning corresponds to a 0V clamp signal.
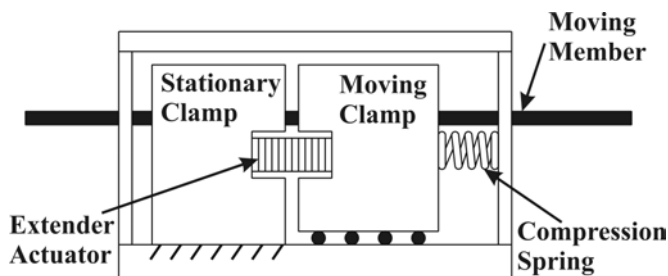

Fig. 1. General complementary inchworm actuator configuration.

Design configurations for the NU and NC clamps are illustrated in Fig. 2 along with the corresponding restraining force vs. applied voltage characteristics assuming a constant coefficient of friction. For the NU clamp of Fig. 2a), a multilayer piezoelectric stack is supported in a flexure frame in order to maintain a moderate pre-stress and protect the stack from shear forces imparted by the moving member. An upper clamping surface is suspended above the moving member and held in place by front and back face-plates (not shown in the figure). The upper section of the clamp has a relatively stiff flexure and a less stiff internal spring that can be compressed by set-screw rotation. Because of the low stiffness ratio between the internal spring and upper flexure, the position of the unobstructed upper clamping surface can be adjusted with micron level control by set-screw rotation. The NU clamp is adjusted so that with zero voltage on the piezoelectric stack, the gap between the two clamping surfaces slightly exceeds the moving member thickness resulting in zero clamping force. The clamping threshold voltage, $V_{TNU,}$ is the piezoelectric stack voltage at which the separation of the two clamping surfaces first equals the moving member thickness. It can be adjusted by set-screw rotation. Beyond $V_{TNU,}$ the restraining force on the moving member begins to rise. The subsequent slope of the restraining force vs. voltage characteristic depends on the properties of the piezoelectric stack, the stiffness of the upper clamping flexure and the coefficient of friction between the moving member and clamping surfaces. The force, F_{MAX}, denotes the maximum restraining force corresponding to the maximum permissible applied voltage for the stack actuator.

Fig. 2b) shows a configuration for the NC clamp. It is essentially the same as the NU clamp of Fig. 2a) except that the piezoelectric stack is oriented horizontally and acts through a Cymbal-style flexure [7]. Cymbal flexures can incorporate amplification at the cost of stiffness [8]. This clamp configuration would be designed to have an amplification of unity in order to have the same F_{MAX} and $|dF/dV|$ of the NU clamp in Fig. 2a). The clamping threshold voltage, V_{TNC}, is the piezoelectric stack voltage at which the clamping surface first separates from the moving member. The designs of Figs. 2a) and 2b) have close to the same mass and either could be used as the moving clamp. The choice will ultimately depend on whether it is preferred to have the moving member fixed to the stationary clamp or subject to fine positioning control when the clamp voltages are zero.

Fig. 2c) shows an alternate NC clamp design in which a piezoelectric stack is used to raise a horizontal bar that clamps on the top of the moving member. This design uses the same flexure frame to house the piezoelectric stack as in Fig. 2a), but the frame is now shown in side view. The restraining force, F_{MAX}, at $V=0$ is established by using the adjustment bolt with a compression spring while the central contact piece is in a raised position. The contact piece can then be locked into contact with the actuator frame with the stack voltage set equal to the value V_o. The slope of the descending portion of the restraining force vs. applied voltage characteristic depends on the properties of the piezoelectric stack, the compliance of the horizontal bar and the coefficient of friction. This design is more massive than Fig. 2b) and is better used as the stationary clamp.
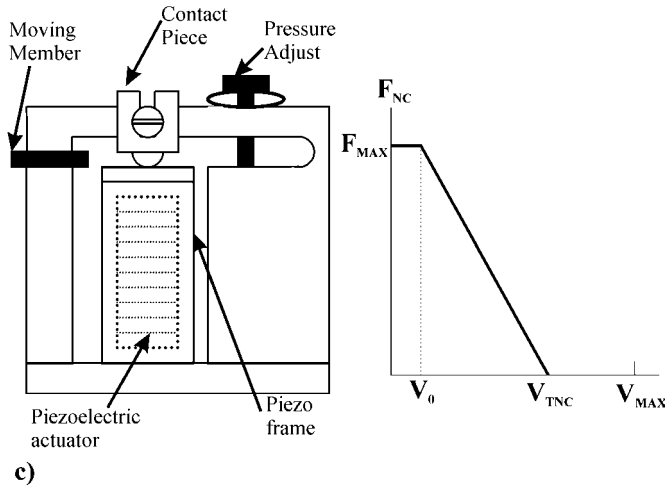

a)

b)

c)
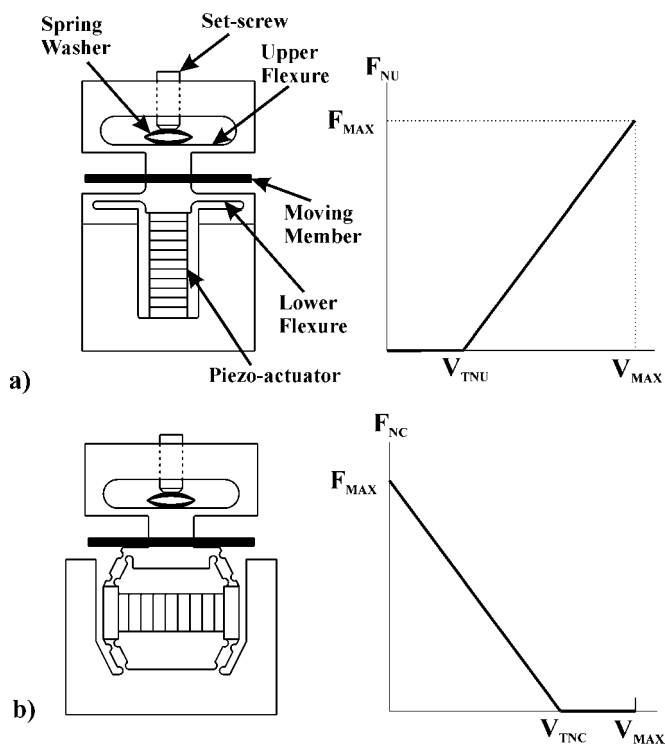
Fig. 2. Clamp configurations with their restraining force-voltage characteristics, a) NU clamp, b) Cymbal-style NC clamp, and c) lever-style NC clamp.

III. DELAY CIRCUIT

In conventional inchworm control, the clamp signals are sequenced with the extender signal such that the clamping clamp is completely engaged before the unclamping clamp begins to release. In the complementary inchworm, unclamping and clamping are occurring at the same time. Fig. 3 shows a general form of the channel signals.
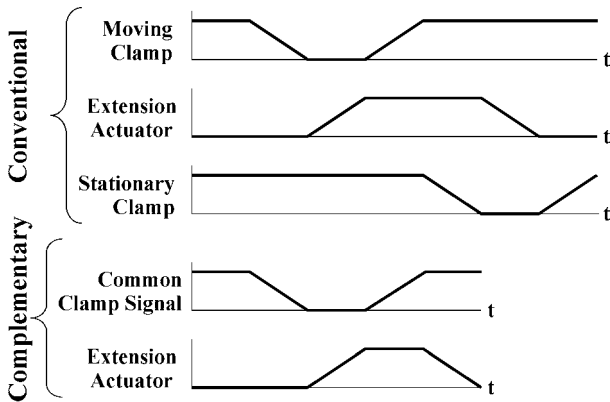

Fig. 3. Inchworm actuator conventional and complementary drive signals.

Fig. 4 shows the total restraining force acting on the moving member (i.e. $F_{NU}+F_{NC}$) and the common clamp input voltage as a function of time for the case of ideal complementary clamps where the force-voltage characteristics of the individual clamps are as shown on the right side of Figs. 2a) and 2b). For the *no delay* curve in the figure, it is assumed for simplicity that the clamps are fully complementary so that the magnitude of the force vs. voltage slopes for the two clamp types are the same and they have the same F_{MAX}. It is also assumed that $V_{TNU}=0.3 \cdot V_{MAX}$, and $V_{TNC}=V_{MAX} - V_{TNU}$. There is no common clamp voltage at which the total restraining force is zero, provided the condition $V_{TNC}>V_{TNU}$ is satisfied. However, the figure shows that the total restraining force is reduced for common clamp voltages that are intermediate between 0 and V_{MAX}. The reduction occurs because of the finite regions of the individual force vs. voltage characteristics where one clamp cannot compensate for force reduction of the other ($V<V_{TNU}$ for the NU clamp and $V>V_{TNC}$ for the NC clamp). These regions cannot be entirely removed from a practical design and we therefore expect that a complementary inchworm actuator with 2-channel control would ordinarily have a lower force drive capability than if the same actuator used 3-channel control to ensure that one clamp is fully on before the other

begins to release.

   Fig. 4 also shows the effect of using a suitable delay circuit that causes the unclamping operation to occur more slowly than clamping. In this case, a linear delay was implemented by reducing the slope of the unclamping voltage signal vs. time by the specified percentage. As the delay increases, the minimum total restraining force, F_{MIN}, increases. It is observed that if the delay is sufficiently large, the total restraining force exceeds F_{MAX} for a short period because the NC force has not yet reached zero when the NU force first reaches F_{MAX}. It is important to ensure that the extender actuator is not triggered until the NC clamp has reached zero force and this means that the delay cannot be made arbitrarily large. Nevertheless, a complementary inchworm actuator with 2-channel control may be able to approach 3-channel performance by using a suitable delay circuit. One such delay circuit is described qualitatively here and is analyzed quantitatively in subsequent sections.
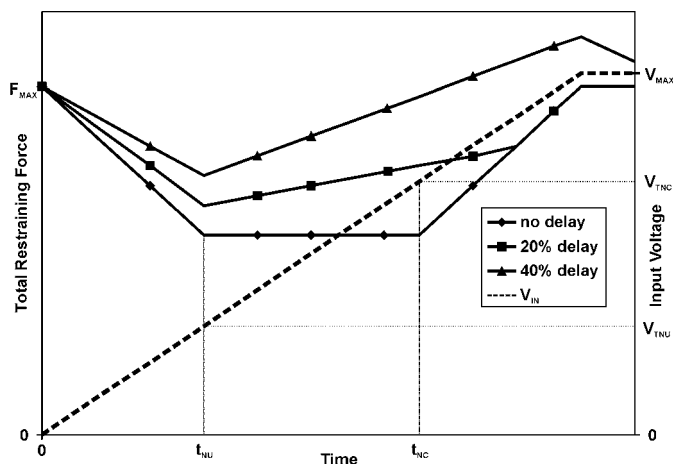

Fig. 4. Total restraining force (solid curves) and common clamp input voltage (dashed curve) vs. time.

   Fig. 5 shows a generic delay circuit connected to each clamp with a common voltage supply. The circuit assumes subresonant operation where the piezoelectric stack actuators can be modeled as simple capacitors having values C_{NU} and C_{NC}. A diode-shunted impedance, $Z_{d,}$, is placed in series with each clamp. The diodes are oriented in different directions so that for each clamp type, the impedance is bypassed during the clamping operation and the clamp voltage closely follows the input signal. However, during unclamping, the diode is reverse biased and behaves as an open circuit. The impedance then influences the output voltage and slows its average ramp rate relative to the input signal.

   In the simplest case, Z_d can be a resistor, $Z_d = R$. This introduces a time constant $\tau = R \cdot C_{NU}$ (and $\tau = R \cdot C_{NC}$) into the system during the unclamping portion of the cycle. As will be shown in subsequent sections, the design value of the resistor, R, involves a tradeoff between increased minimum restraining force during the switching transient and power loss in R. Higher order reactive circuits involving inductive and capacitive elements may also be used for Z_d[6] and the circuit in Fig. 6 was chosen in order to investigate its performance. It is shown in Section VI that the purely resistive circuit has the best performance and consequently the effect of resistance is the main focus of testing and analysis.
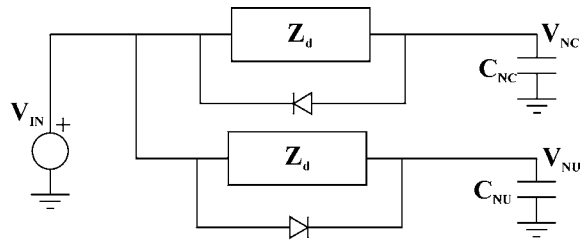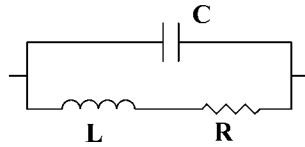
Fig. 5. Generic delay circuit.

Fig. 6. Impedance circuit used in Z_d blocks of Fig. 5 for simulation and experiment.

IV. CLAMP MODEL

The model of the clamp is composed of coupled electrical and mechanical sub-models. The mechanical model for the NU clamp from Fig. 2a) is considered and has fully complementary characteristics as the clamp from Fig. 2b) if its amplification is unity. The clamp can be represented as shown in Fig. 7. The piezoelectric stack, upper spring, lower flexure and upper flexure have stiffnesses k_p, k_s, k_f and k_{fa} respectively. The lower flexure has a clearance, C_r, to the moving member at $V=0$. The clamping force, F_c, is the net result of the piezoelectric stack force, F_p, and the lower flexure force, F_f.
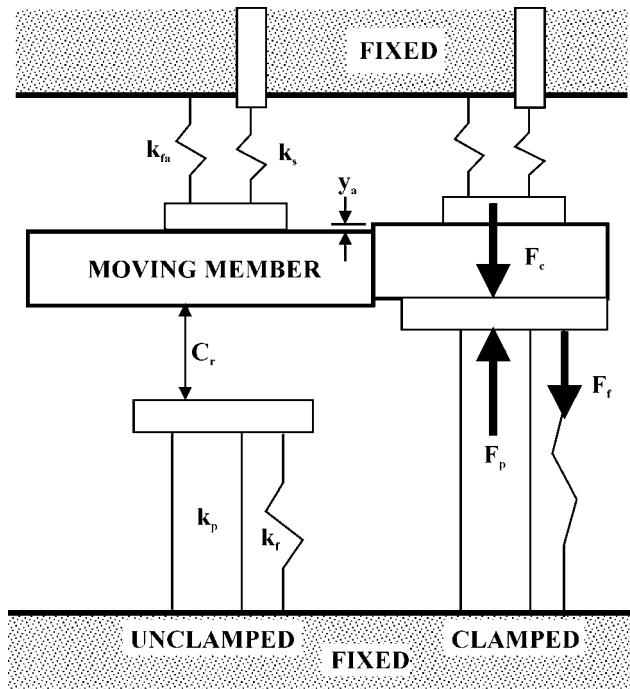

Fig. 7. NU clamp representation in the unclamped ($V=0$) and clamped ($V>V_{TNU}$) states.

Using equations developed previously[9] and also shown in the Appendix, the clamping force can be calculated as a function of piezoelectric stack voltage, V, and clearance:

$$F_c = \begin{cases} \dfrac{k_s + k_{fa}}{k_p + k_f + k_s + k_{fa}}\left(k_p \dfrac{L_0}{V_{MAX}}V - \left(k_p + k_f\right)C_r\right) & V > V_{TNU}. \\[2em] 0 & V \le V_{TNU}. \end{cases} \qquad (1)$$

The threshold voltage, V_{TNU}, is

$$V_{TNU} = \frac{C_r(k_p + k_f)}{L_0 k_p}V_{MAX}. \qquad (2)$$

L_0 is the free expansion of the piezoelectric stack at maximum voltage V_{MAX}. These equations give the relationship of the force-voltage characteristic in Fig. 2a) where F_c and the restraining force F_{NU} are related by the coefficient of friction. The maximum clamping force which can be realized is

$$F_{cMAX} = \frac{k_s + k_{fa}}{k_p + k_f + k_s + k_{fa}}\left(k_p L_0 - \left(k_p + k_f\right)C_r\right). \qquad (3)$$

These equations are based on a static analysis and neglect hysteresis and other dynamic effects.

The electrical model relates the clamp voltages to the input voltages which depends on the particular impedance circuit used. For the *RLC* circuit in Fig. 6, the transfer function is given by

$$V_{NU,NC} = \begin{cases} \dfrac{s^2 CL + sCR + 1}{s^2 L(C + C_{NU,NC}) + sR(C + C_{NU,NC}) + 1}V_{IN} & \begin{array}{l} delay \\ active \end{array} \\[2em] V_{IN} & \begin{array}{l} diode \\ active. \end{array} \end{cases} \qquad (4)$$

V. EXPERIMENTAL RESULTS

The stack actuators considered in this work have area 5 mm x 5 mm, height 11 mm and a low frequency capacitance of approximately 430 nF. The displacement of the stacks at the rated maximum voltage (200 V) is just over 12 μm.

Tests were conducted on a prototype clamp with a diode-shunted delay circuit with the impedance shown in Fig. 6 to assess the clamping force and resistive loss. Clamping force is easier to consistently measure than the restraining force which is why it is considered here. The lower frame with stack actuator (lower section of Fig. 2a) was mounted in a test fixture and the base secured. The voltage signal was generated by an arbitrary waveform generator. The signal passed through an amplifier and into the diode-shunted delay circuit which controlled the clamp. The voltage signal profile was a step with ramped edges at a frequency of 200 Hz. A quartz load cell with a stiffness of 1000 N/μm was placed on top of the clamp surface. An upper flexure was fastened a distance C_r above the load cell. The input voltage, clamping force, and current in the *RL* branch were monitored in real time using a digital sampling oscilloscope.

Fig. 8 shows the experimental results of the NU clamping force for various *RL* branch resistances. The clamp force is shown as a function of time for the case when the input voltage was ramped from 0 V to 200 V in 1 ms, held constant for 2.5 ms, and then ramped down to 0 V in 1 ms. The curves with delay circuit use C=100 nF, L=1 mH, and R values as shown. The figure shows that the rate of change of force during unclamping is slowed by the delay circuit and that a greater R reduces the rate by a larger amount. While the amount of resistance does not affect the rate during clamping, the rising portion of the force curve was not linear even though the input voltage ramp was. This is due to hysteresis and other dynamic effects in piezoelectric actuators which are dependent on frequency[10]. The oscillation at the top of the force curve is due to a resonance in the test fixture and could not be eliminated through filtering, but is not intrinsic to the clamp design.
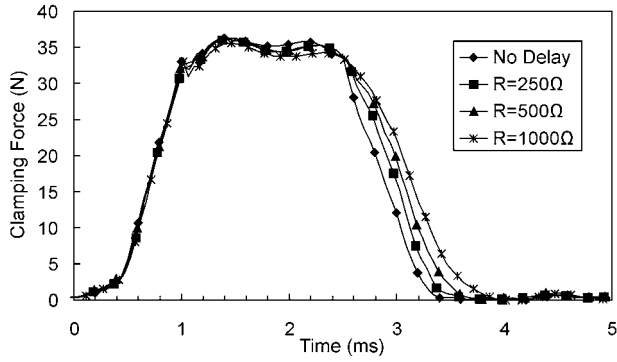
Fig. 8. Experimental results showing NU clamping force vs. time for various resistances in the delay circuit.

To estimate the total restraining force profile of the inchworm, the NC clamp signal was inferred from the results from Fig. 8 assuming an NC clamp of Fig. 2b) with force characteristics fully complementary to the NU clamp. The coefficient of friction was assumed to be unity for simplicity. The force curve was shifted and then the total restraining force was obtained by the addition of the force profiles of the NU and NC clamps. The results are shown in Fig. 9 as the common clamp voltage is ramped from 0 to 200V at a rate of 200V/ms. It can be seen that increasing the resistance increases the minimum restraining force, F_{MIN}. There are no distinct transition points where the different clamps activate and deactivate as would be expected from Fig. 4. This is due to nonlinear effects that cause the rising portion of the clamp force profile to have a smooth instead of a sharp transition at V_{TNU}.
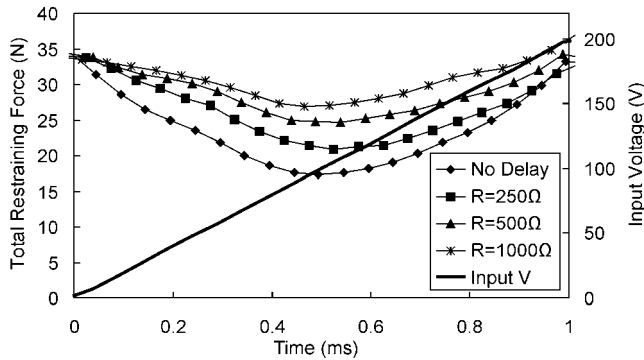

Fig. 9. Inferred results showing total restraining force vs. time for various resistances in the delay circuit.

VI. COMPARISON OF EXPERIMENTAL RESULTS TO SIMULATION

The simulation will be used as a design tool to optimize designs before they are constructed. In this section, the simulation model is compared to the experimental results in order to validate the model's performance. PSPICE[11] was used to simulate the voltage applied to the piezoelectric stacks using the circuits shown in Figs. 5 and 6. Given the same values for C, L, R, C_{NC}, and C_{NU} used in the experiments, the voltages across C_{NC} and C_{NU} were determined. To obtain the clamping force from the voltages, the intercept, V_{TNU}, and the slope from Fig. 2a) were inferred from a test of the clamp without the delay circuit (see Fig. 10). The test also exhibits nonlinear effects so an average of the rising and falling slopes was used. The coefficient of friction was taken as unity as before.
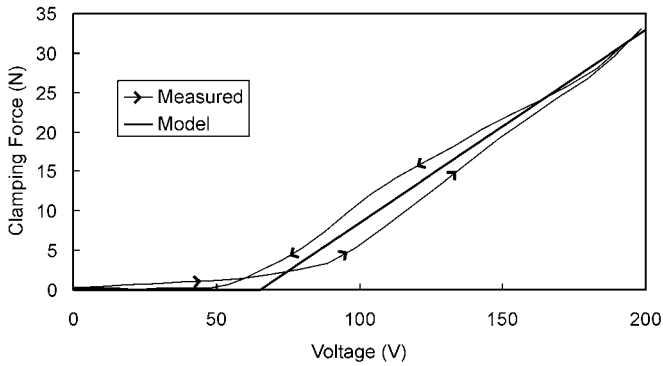
Fig. 10. Measured clamping force as a function of voltage and model used in simulation.

Fig. 11 shows the simulated total restraining force of the inchworm actuator as a function of time as the common clamp voltage is ramped from 0 to 200 V at a rate of 200 V/ms. The results show clearly identifiable transition points which are the times when the input voltage is equal to V_{TNU} and V_{TNC}.
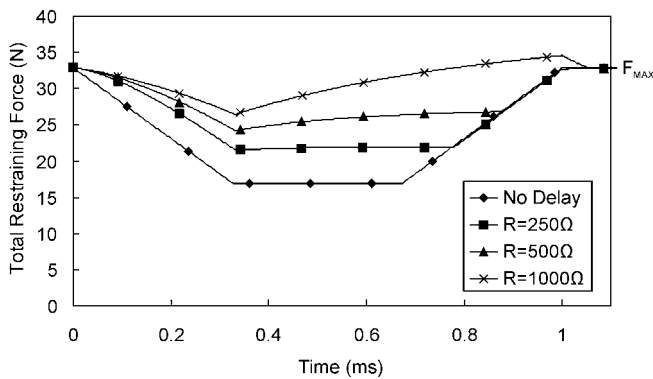

Fig. 11. Simulated total restraining force vs. time for complementary inchworm actuator with and without diode-shunted delay circuit.

It is observed that for R=1000 Ω, the total restraining force exceeds F_{MAX} for a short period since the NC clamp is not fully released when the NU clamp reaches its maximum force. Therefore, above this value of R, the extender signal would need to be delayed to ensure unclamping is complete. Note that in the experimental results for R=1000 Ω, F_{MAX} has not been exceeded (Fig. 9). This is due to nonlinear effects delaying the rising portion of the force curve which is not present in the simulation. Therefore, we could use a larger R than indicated by the simulation without having to modify the extender signal profile.

Fig. 12 shows the comparison of F_{MIN} and the power loss in R vs. resistance, R, for the simulation and experimental results. The simulation, ignoring nonlinear effects, provides good agreement with the measured F_{MIN} but underestimates the power loss in R.
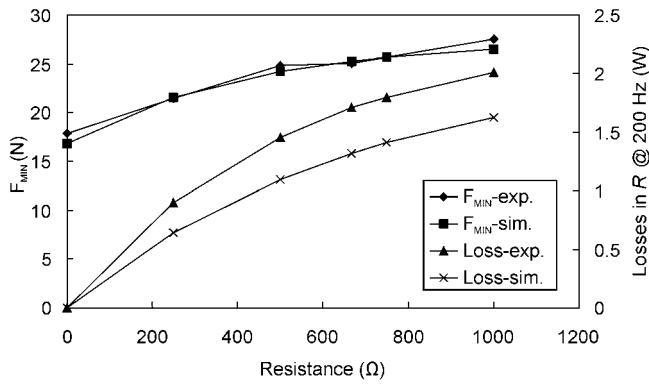
Fig. 12. Comparison of F_{MIN} and power loss in R vs. resistance, R, for the simulation and experimental results.

Fig. 13 shows the simulated effect of the other parameters in the RLC circuit. It is observed that the highest F_{MIN} for a given power loss is achieved by the purely resistive circuit.
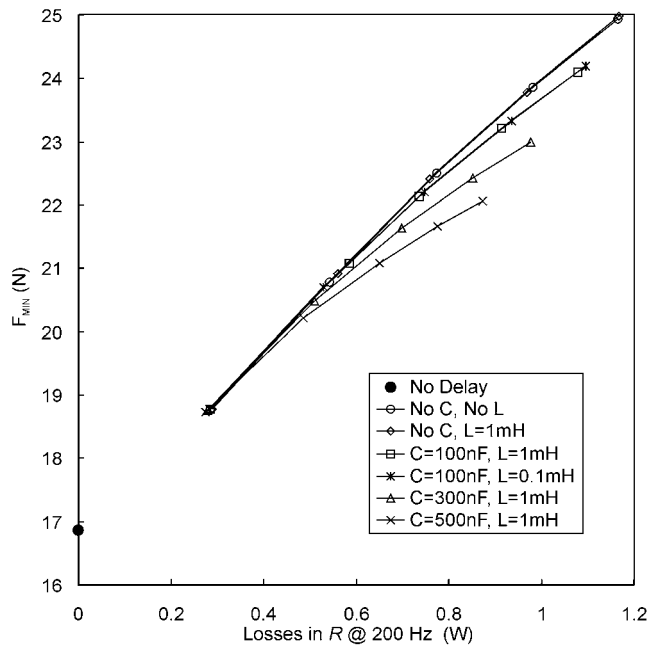

Fig. 13. Simulation results showing the effect of C and L on the performance of the delay circuit.

VII. CONCLUSIONS

Novel complementary clamp configurations for inchworm actuators have been described which allow one control signal to drive both clamps. This is achieved by designing the clamps so that one releases at high voltage and the other at low voltage.

A diode-shunted delay circuit has also been described which selectively slows the rate of unclamping relative to clamping. It has been shown by experiment and simulation that the circuit increases the actuator total restraining force during the clamp switching transient. The complementary inchworm actuator with 2-channel control can achieve close to the same force drive capability as a comparable inchworm actuator using 3-channel control.

A simple resistive impedance, $Z_d=R$, had better performance than a more complex RLC circuit. Delay and minimum total

restraining force increase as R increases at the cost of increased power loss.

This appendix shows the derivation the equations for the clamp model of Section IV. From [12] the force of the piezoelectric stack, F_p, can be written as a function of its stiffness, k_p, free expansion , L_0, maximum voltage, V_{MAX}, and its displacement, δ_p.

$$F_p = \left(\frac{L_0}{V_{MAX}} V - \delta_p \right) k_p \tag{A1}$$

The total displacement of the piezoelectric stack is a combination of the displacement to cover the gap, C_r, and the deflection of the upper flexure, y_a.

$$\delta_p = C_r + y_a \tag{A2}$$

Combining (A1) and (A2) gives F_p.

$$F_p = \left(\frac{L_0}{V_{MAX}} V - C_r - y_a \right) k_p \tag{A3}$$

The force balance in the vertical direction gives the relation of the clamping force, F_c, piezoelectric stack force, and the lower flexure force, F_f.

$$F_c = F_p - F_f \tag{A4}$$

Using the equation for a linear spring, the lower flexure force can be written as a function of its stiffness, k_f, and its displacement.

$$F_f = k_f (C_r + y_a) \tag{A5}$$

Similarly, the clamping force is related to the upper flexure stiffness, k_{fa}, the spring stiffness, k_s, and its displacement.

$$F_c = (k_{fa} + k_s) y_a \tag{A6}$$

Substituting (A3) and (A5) into (A4) gives (A7).

$$F_c = \left(\frac{L_0}{V_{MAX}} V - C_r - y_a \right) k_p - k_f (C_r + y_a) \tag{A7}$$

Rearranging (A6) for y_a and substituting into (A7) gives F_c.

$$F_c = k_p \frac{L_0}{V_{MAX}} V - (k_p + k_f) C_r - \frac{(k_p + k_f)}{(k_s + k_{fa})} F_c \tag{A8}$$

Solving for F_c gives (A9) which is (1) in Section IV.

$$F_c = \frac{k_s + k_{fa}}{k_p + k_f + k_s + k_{fa}} \left(k_p \frac{L_0}{V_{MAX}} V - (k_p + k_f) C_r \right) \tag{A9}$$

To get the threshold voltage, V_{TNU}, set $V=V_{TNU}$ and $F_c=0$ in (A9) and solve for V_{TNU}. This is (2) in Section IV.

$$V_{TNU} = \frac{C_r (k_p + k_f)}{L_0 k_p} V_{MAX} \tag{A10}$$

For the maximum clamping force, F_{cMAX}, set $F_c=F_{cMAX}$ and $V=V_{MAX}$ in (A9). This is (3) in Section IV.

$$F_{cMAX} = \frac{k_s + k_{fa}}{k_p + k_f + k_s + k_{fa}} \left(k_p L_0 - (k_p + k_f) C_r \right) \tag{A11}$$

REFERENCES

[1] B. Zhang and Z. Zhu, "Developing a linear piezomotor with nanometer resolution and high stiffness," *IEEE/ASME Trans. on Mechatronics*, vol. 2, pp.22-29, 1997.
[2] R. Ben Mrad, A. Abhari and J. Zu, "A control methodology for an inchworm piezomotor," *J. of Mechanical Systems and Signal Processing*, vol. 17, pp. 457-71, 2003.
[3] J. Kim; J-D. Kim and S-B Choi, "A Hybrid Inchworm Linear Motor," *Mechatronics*, vol. 12, pp. 525-42, 2002.
[4] A. Suleman, S. Burns, D. Waechter, R. Blacow, B. Yan and S.E. Prasad, "Flexural brake mechanism for inchworm actuator," *Proc. Canada-US CanSmart Workshop on Smart Materials and Structures*, Montreal, 2001, pp. 125-136.
[5] R. Yeh, S. Hollar and K.S.J. Pister, "Single mask, large force, and large displacement electrostatic linear inchworm motors," *J. of Microelectromechanical Systems*, vol. 11, pp.330-336, 2002.

[6] D. F. Waechter, S. Salisbury, R. Ben Mrad, S. Eswar Prasad, R. G. Blacow, and B. Yan, "Complementary inchworm actuator for high-force high-precision applications," *Proc. SPIE Smart Structures And Integrated Systems*, vol 5390, San Diego, March 2004.

[7] A. Dogan, K. Uchino, and R. E. Newnham, "Composite piezoelectric transducer with truncated conical endcaps cymbal," *IEEE Trans. on Ultrasonics, Ferroelectrics, and Frequency Control*, vol. 44, no. 3, pp. 597-605, May 1997.

[8] P. E. Tenzer and R. Ben Mrad, "On amplification in inchworm precision positioners," *Mechatronics*, vol. 14, issue 5, pp. 515-531, June 2004.

[9] S. Salisbury, D. Waechter, R. Ben Mrad, R. Blacow and E. Prasad, "Design tools for piezoelectric actuated inchworm positioners," *Proc. Canada-US CanSmart Workshop on Smart Materials and Structures*, Montreal, 2003, pp. 169-175.

[10] R. Ben Mrad and H.Hu, "A model for voltage-to-displacement dynamics in piezoceramic actuators subject to dynamic –voltage excitations," *IEEE Trans. on Mechatronics*, vol. 7, no. 4, pp. 479-489, Dec. 2002.

[11] PSPICE, Version 9.1, Cadence Design Systems Inc.

[12] *IEEE Standard on Piezoelectricity*, ANSI/IEEE Standard 176-1987.